NANO FUTURES

LETTER

Scalable nanomanufacturing and assembly of chiral-chain piezoelectric tellurium nanowires for wearable self-powered cardiovascular monitoring

RECEIVED
10 October 2018

ACCEPTED FOR PUBLICATION
10 December 2018

PUBLISHED
4 January 2019

Yixiu Wang[1,2], **Ruoxing Wang**[1,2], **Shihan Wan**[3], **Qingxiao Wang**[4], **Moon J Kim**[4], **Dong Ding**[5] and **Wenzhuo Wu**[1,2,6,7]

[1] School of Industrial Engineering, Purdue University, West Lafayette, IN 47907, United States of America
[2] Flex Laboratory, Purdue University, West Lafayette, IN 47907, United States of America
[3] School of Mechanical Engineering, Purdue University, West Lafayette, IN 47907, United States of America
[4] Department of Materials Science and Engineering, University of Texas at Dallas, Richardson, TX 75080, United States of America
[5] Energy & Environment Science and Technology, Idaho National Laboratory, Idaho Falls, ID 83415, United States of America
[6] Birck Nanotechnology Center, Purdue University, West Lafayette, IN 47907, United States of America
[7] Regenstrief Center for Healthcare Engineering, Purdue University, West Lafayette, IN 47907, United States of America

E-mail: wenzhuowu@purdue.edu

Keywords: piezoelectric device, scalable nanomanufacturing, tellurium nanowires, self-powered sensor, wearable electronics, physiological monitoring

Supplementary material for this article is available online

Abstract

The economically viable production of piezoelectric nanomaterials that can efficiently convert low-level mechanical signals into electrical power promises to revolutionize the emerging self-powered technologies in wearable sensors, consumer electronics, and defense applications. Here, we report the scalable nanomanufacturing and assembly of tellurium (Te) nanowires with chiral-chain structure into wearable piezoelectric devices, and explore the feasibility of such devices for self-powered sensing applications, e.g. cardiovascular monitoring. The ultrathin device can be conformably worn onto the human body, effectively converting the imperceptible time-variant mechanical vibration from the human body, e.g. radial artery pulse, into distinguishable electrical signals through straining the piezoelectric Te nanowires. We further uncover the process-structure-property relationships in designing, manufacturing, and integrating the Te nanowire piezoelectric devices. Our results suggest the potential of solution-synthesized Te nanowire as a new class of piezoelectric nanomaterial for self-powered devices and may lead to new opportunities in energy, electronics, and sensor applications.

The capability of functional devices to sense, process, interact, and communicate with the acquired information carried by the signals from the environment (e.g. the human body), such as vibration and temperature, enables a multitude of emerging technologies, e.g. wearable electronics, artificial skins, and smart medical devices. Although non-electrical signals such as mechanical stimuli are ubiquitous and abundant in these applications, the electrically-controlled operation scheme in existing technologies requires a complex integration of heterogeneous components to interface the mechanical signals in the working environment. Moreover, the requirement of the power source (e.g. batteries) further complicates the system design for implementing the ubiquitous applications.

The conversion of mechanical stimuli into electrical signals can be achieved through various mechanisms, e.g. electromagnetic induction [1], electrostatic generation [2], contact triboelectrification [3], and piezoelectricity [4]. The harvesting of mechanical energy using nanostructured piezoelectric materials has particular technology appeal and recently received considerable attentions [4–20] due to the direct conversion process which is feasible for integrated applications and its versatility in efficiently harvesting ubiquitous mechanical energy, hinged on principles of the time-variant piezoelectric polarization induced displacement

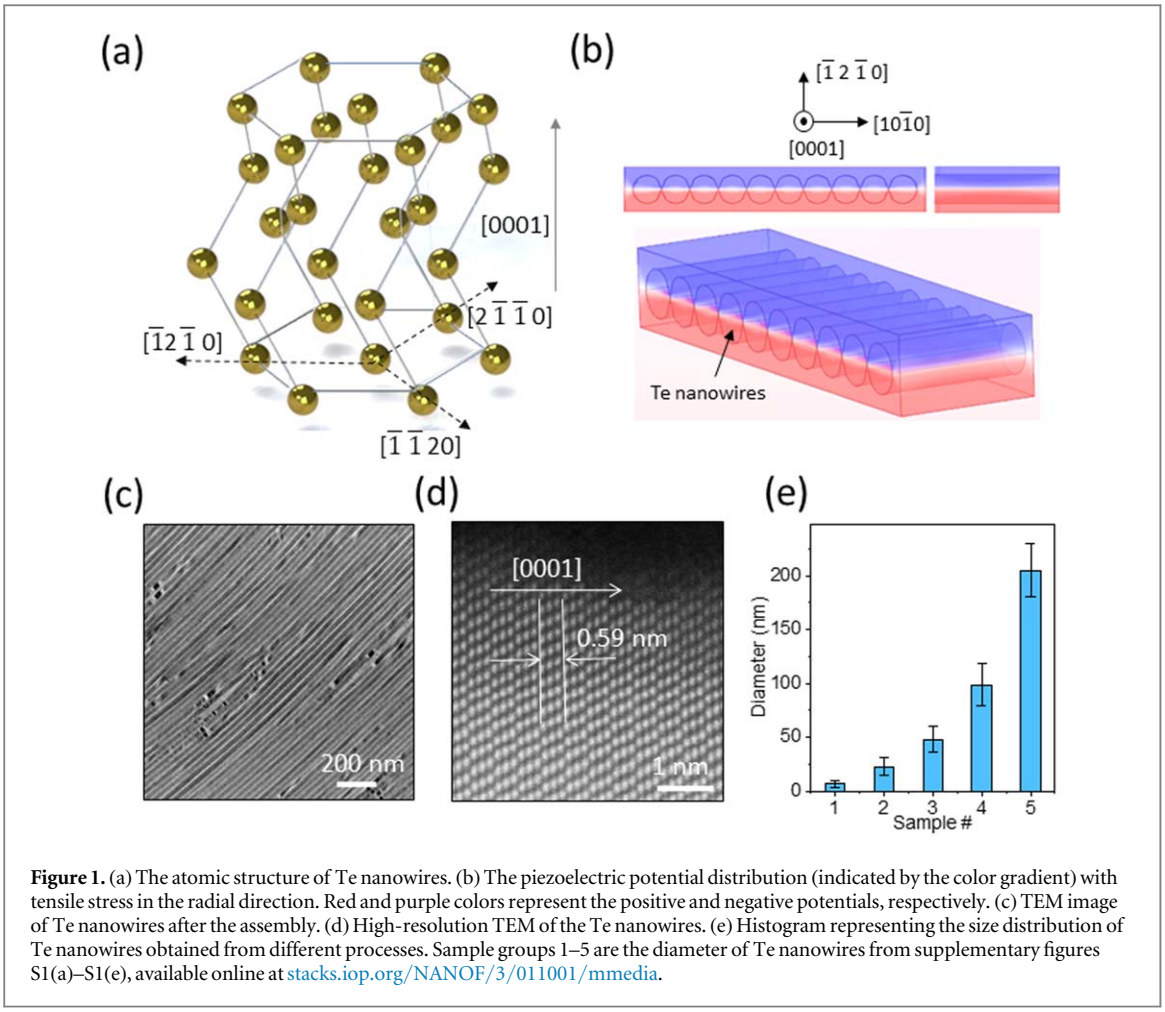

Figure 1. (a) The atomic structure of Te nanowires. (b) The piezoelectric potential distribution (indicated by the color gradient) with tensile stress in the radial direction. Red and purple colors represent the positive and negative potentials, respectively. (c) TEM image of Te nanowires after the assembly. (d) High-resolution TEM of the Te nanowires. (e) Histogram representing the size distribution of Te nanowires obtained from different processes. Sample groups 1–5 are the diameter of Te nanowires from supplementary figures S1(a)–S1(e), available online at stacks.iop.org/NANOF/3/011001/mmedia.

current [21]. Moreover, the low-dimensional geometries and superior mechanical properties of piezoelectric nanomaterials compared to their bulk counterparts facilitate the integration into flexible devices that can potentially sustain large strain [22, 23]. Ongoing efforts in the field of piezoelectric nanodevices are primarily focused on augmenting power generation by further improving the materials' piezoelectric and mechanical characteristics [24–26], engineering the dielectric environment [26, 27], optimizing the properties of contact interface [28], and demonstrating proof-of-concept application [29]. Progress in these fields combined with the emerging methods for deterministic production and assembly of nanomaterials [26] leads to exciting research opportunities. Nevertheless, significant roadblocks exist against the demonstrated piezoelectric nanodevices from realizing their technological potential. There is a lack of options for scalable manufacturing and integrating piezoelectric nanomaterials at a high-production rate and with good reproducibility. Obstacles concerning scalable, economical production of related materials such as the intricate fabrication and expensive machinery continue to prevail.

Here we demonstrate the first scalable nanomanufacturing and integration of tellurium (Te) nanowires into wearable piezoelectric devices and explore the feasibility of such devices for self-powered sensing applications, e.g. cardiovascular monitoring. The ultrathin device can be conformably worn onto the human wrist, effectively converting the pulse-induced imperceptible time-variant mechanical vibration into distinguishable electrical signals, which are the polarization induced displacement current [30], through straining the piezoelectric Te nanowires. We further identified the correlation between the piezoelectric outputs from the integrated devices and the process-controlled structural properties, e.g. diameters, of Te nanowires by revealing the process-structure-property-performance relationship for the solution-nanomanufactured Te nanowire wearable piezoelectric devices, which is expected to guide nanomanufacturing and practical application of other piezoelectric nanomaterials.

The trigonal-structured Te has an anisotropic crystal lattice where individual chiral chains of Te atoms are stacked together by weak bonding [31–34] (figure 1(a)). Each Te atom is covalently bonded with its two nearest neighbors on the same chain. Despite that the structure of Te is non-centrosymmetric, few studies have been reported on the piezoelectricity in bulk Te [35, 36], possibly due to its narrow bandgap (~0.35 eV) as a result of the lone-pair and anti-bonding orbitals [37, 38]. Recent research shows that nanostructured tellurium could

exhibit strong piezoelectric property [7], leading to a potential high volume-power-density in integrated devices. Furthermore, the radial distribution of piezoelectric polarization [7] in the Te nanowire (figure 1(b)), due to the strain-induced relative displacement of the electron distribution against the Te atoms cores [39], facilitates its integration into ultrathin laminated devices through economic manufacturing approaches, e.g. roll-to-roll printing, onto various substrates [40].

Despite that a wealth of solution-phase synthetic methods have been developed for synthesizing Te nanowires [41], the scalable production and rational assembly of Te nanowires with controlled dimensions (in particular the diameter) and properties remain underexplored [42]. In this article, we report a substrate-free solution process for manufacturing large-scale, high-quality Te nanowires with controlled diameters (figure 1(c), supplementary figure S1). The samples are grown through the reduction of sodium tellurite (Na_2TeO_3) by hydrazine hydrate (N_2H_4) in an alkaline solution at temperatures from 160 °C to 200 °C, with the presence of crystal-face-blocking ligand polyvinylpyrrolidone (PVP) (see Methods) [43]. Due to the hydrophilic nature, the Te nanowires can be transferred and assembled at large-scale into a single layer continuous thin film through a Langmuir–Blodgett (LB) process [44] (Methods) for device integration and characterization. Figure 1(c) shows the low-magnification transmission-electron-microscopy (TEM) image of a such LB film of Te nanowires with uniform diameters. Figure 1(d) shows a typical atomically-resolved high angle annular dark field scanning TEM (HAADF-STEM) image of the Te nanowires. The chiral chains and a threefold screw symmetry along $\langle 0001 \rangle$ are visible, with a corresponding interplanar spacings of 5.9 Å (figure 1(e)) [34].

The diameter of as-synthesized Te nanowires can be controlled through modulation of the synthesis processes. To achieve this, we adopted an alkaline reaction condition (Methods) where the standard electromotive force (EMF) is smaller than that for an acid media [45]. The consequent slower reduction process enables the uniform morphology of the as-derived Te nanowires (figure 1(d)). We found that the solvent also plays a critical role in controlling the diameter of Te nanowires (supplementary figure S1, supplementary table 1). Samples with the smallest diameter (7 ± 3 nm) can be derived when pure deionized (DI) water was used as the solvent. The diameters of the as-synthesized nanowires increased to 23 ± 8 nm when half of the DI water was replaced by ethylene glycol (EG). Thicker Te nanowires (48 ± 12 nm) were obtained when pure EG was used as the solvent. This can be understood by examining the different solubility of PVP in DI water and EG [46]. The solubility of PVP in EG is much smaller than that in water [46], which leads to the partial polymer collapse of PVP on the surface of the as-formed Te crystals in EG during the growth. As a result, the insufficient passivation of PVP on Te in EG allows the Te nanowire grow fast along the radial direction with larger diameters. To further prove this, we introduced acetone, in which PVP has even poorer solubility than in EG [46], into the solvent. As is shown in supplementary figures S1(d), (e), the diameter continuously increases with the increase of the amount of acetone. However, too much acetone (supplementary figure S1(f)) will result in the thick and short nanostructures with irregular shapes.

We further examined and identified the correlation between the piezoelectric outputs at the integrated devices level and the process-controlled diameters of Te nanowires at the material level, by revealing the process-structure-property-performance relationship for the solution-nanomanufactured Te nanowire wearable piezoelectric devices. Such knowledge will enable the future modeling, design, and processing of Te nanowires for high-performance piezoelectric devices. The detailed process for fabricating the flexible piezoelectric device based on Te nanowires is shown in the experimental section. The device (figure 2(a)) consists of multiple layers stacking of ITO/PET, Te nanowires, and polydimethylsiloxane (PDMS). Figure 2(b) shows the excellent deformability of our Te piezoelectric device which can withstand large degrees of mechanical deformation without fracture or cleavage. Tapping-mode atomic force microscopy (AFM) was used to examine the assembled Te nanowires, showing that uniform Te nanowires with high aspect ratio exceeding 1000:1 were assembled into a continuous monolayer film at large-scale (figure 2(b)). The high aspect ratio and small diameter of Te nanowires are beneficial for improving the device's mechanical robustness and deformability [47]. The typical results of piezoelectric current and voltage output from devices made of Te nanowires with 7 ± 3 nm diameter are shown in figure 2(c) and supplementary figures S2 respectively. Statistical results for the piezoelectric outputs from Te nanowires with different diameters are shown in figure 2(d) and supplementary figures S3. A clear strain-dependent piezoelectric output can be seen for devices made of nanowires with the same diameters (figure 2(c) and supplementary figures S2), consistent with the previously reported results [48]. More interestingly, we also observed a strong dependence of the piezoelectric output on the nanowire diameters (figure 2(d) and supplementary figure S3-4): the output voltage and current increase with the decreased Te nanowire diameters. Such a size-dependent piezoelectric output agrees well with the reported computational results for other piezoelectric nanomaterials, e.g. ZnO and GaN nanowires [49, 50], which is likely due to the size-dependent mechanical (e.g. Young's modulus) [49], piezoelectric (e.g. piezoelectric constant), semiconductor (e.g. bandgap) [34, 51, 52], and other physical properties for 1D nanomaterials [53]. A stable peak power density of 1.06 μW m^{-2}, comparable to reported results [54–56], was obtained for devices built with the thinnest Te nanowires (figure 2(e) and supplementary figures S5). For the remainder of the device

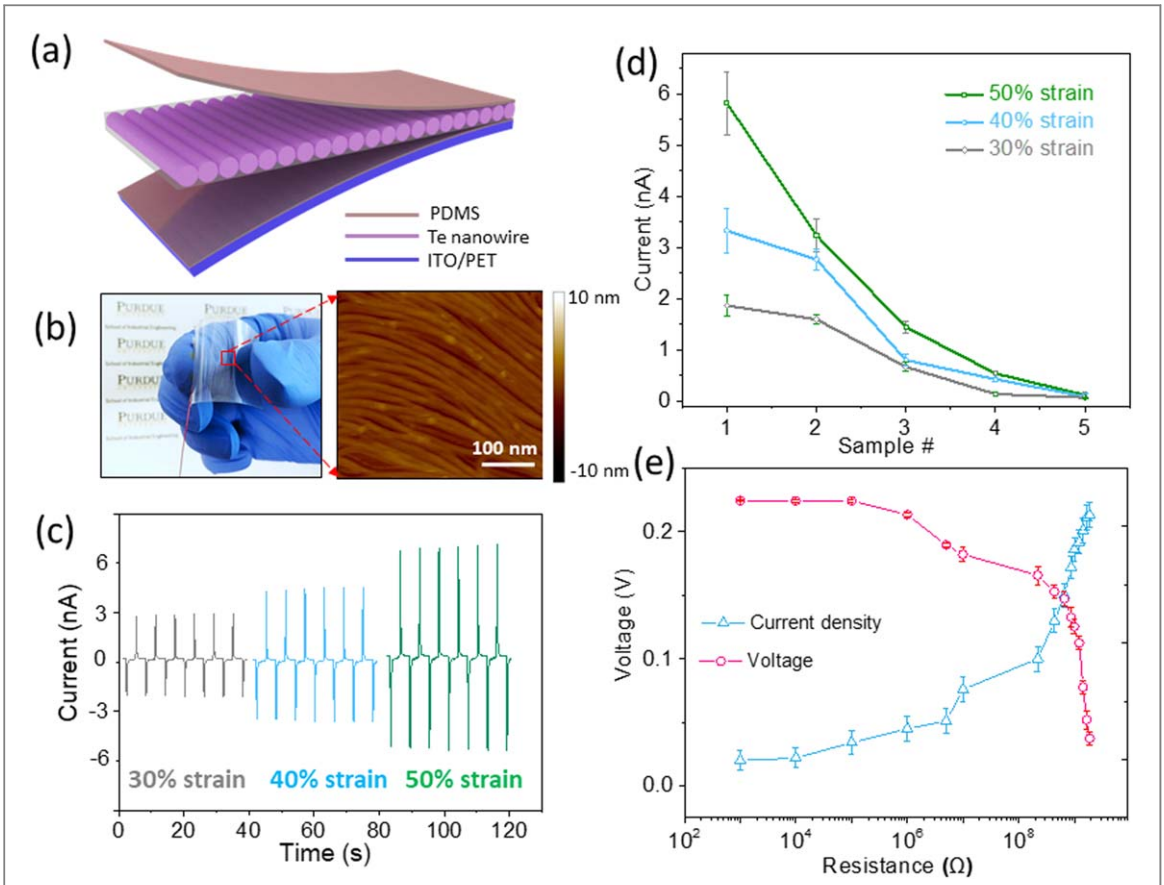

Figure 2. (a) Schematic illustration of the flexible piezoelectric device's structure. (b) Optical image and atomic force microscope (AFM) image of the device surface after assembly. (c) The piezoelectric current output for the thinnest Te nanowires under different strains. (d) Current output of the piezoelectric devices built with Te nanowires with different diameters. (e) The output voltage (left axis) and output current density (right axis) as the function of the load resistance.

characterization and demonstration, we will use one layer of Te nanowires with 7 ± 3 nm diameter in the length of ~50 μm since they provide the highest piezoelectric outputs.

The development of stretchable piezoelectric devices is highly desirable for many emerging technologies, e.g. wearable devices [57]. Our results presented in figure 2 show that the Te nanowires flexible device can withstand 50% uniaxial strain without failure. To fabricate stretchable Te nanowire devices, we directly printed liquid metal (LM) electrodes on the stretchable silicone substrates as the top and bottom electrodes (figure 3(a), Methods). Here we chose Galinstan (a eutectic alloy with the composition ratio of Ga:68.5%, In:21.5%, and Tin:10%) as the LM due to its low melting point (15 °C), high electrical conductivity, low viscosity, and low toxicity [58]. The printed LM electrode shows excellent mechanical stretchability and maintains good electrical conductivity when being subjected to large deformations (figures 3(a), (b)). Due to the excellent mechanical stretchability of all constituents, the Te nanowire stretchable device can convert complex straining (e.g. large-angle twisting in figure 3(a), and hybrid twisting-stretching in supplementary figure S6(b)) into electrical power and sense these mechanical deformations. Our characterization results (figure 3(c), supplementary figure S6(b)) show that the piezoelectric outputs of the Te nanowire stretchable devices increase when we increase the twisting angle and/or the stretching. Moreover, the Te nanowire stretchable device can sense bi-axial strains when being attached to complex surfaces (e.g. the surface of an inflated balloon catheter in figure 3(d) inset). The ultrathin nature of the Te nanowire stretchable device enables its conformal coverage on the balloon surface during the deflation/inflation process (figure 3(d) inset), which is controlled by a linear motor and an attached syringe pump (supplementary figure S7(a)). By tuning the moving speed and distance of the linear motor, we can precisely control the inflating rate of the balloon catheter. The bi-axial in-plane strains (figure 3(d) inset) induced in the Te device during the balloon inflation can result in compression along the $\langle \bar{1}2\ \bar{1}0 \rangle$ direction of the Te nanowire and leads to the piezoelectric polarization (figure 1(b)). Figure 3(d) shows the statistic output voltage and current (supplementary figures S7(b), (c)) with different inflating rates, which can be used to sense and estimate the mechanical deformation/strain on the balloon surface during the operation.

Finally, we explored the feasibility of Te nanowire stretchable device for potential self-powered physiological sensing applications, e.g. cardiovascular monitoring. The wearable device can be attached to the human body

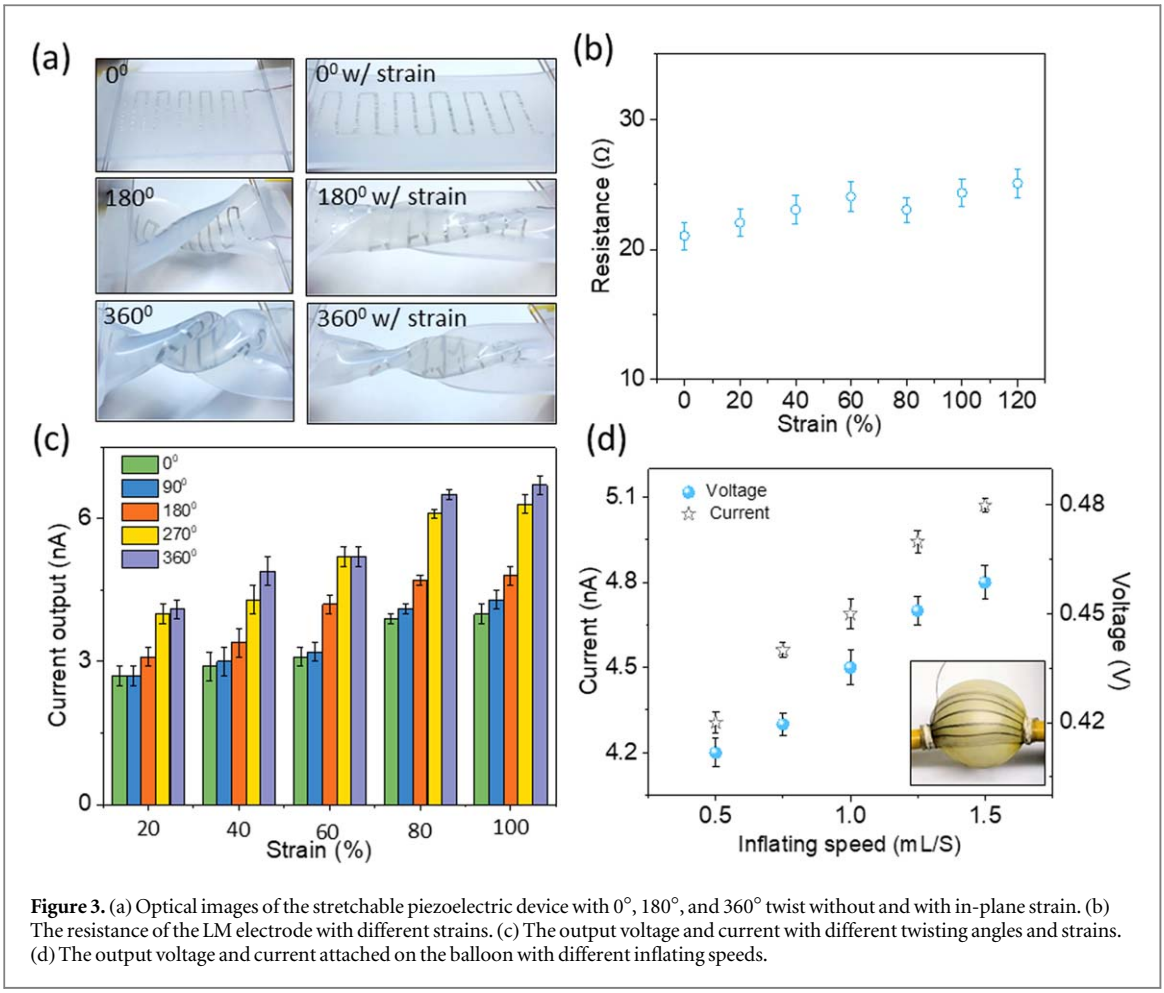

Figure 3. (a) Optical images of the stretchable piezoelectric device with 0°, 180°, and 360° twist without and with in-plane strain. (b) The resistance of the LM electrode with different strains. (c) The output voltage and current with different twisting angles and strains. (d) The output voltage and current attached on the balloon with different inflating speeds.

compliable with minimum deformation. Figure 4(a) shows the application of the device attached to the wrist of a healthy 30 year-old male for the non-invasive detection of pulse without using an external power source. The real-time piezoelectric current output from the device for 30 s shows the reliable detection and measurement of the human pulse signals, with distinct three-peak characteristics for the cardiac cycle (figure 4(b)). Such a pattern is consistent with the reported results [59, 60] and manifests important information for the health diagnostics. Here we attempted to analyze the acquired signals. Specifically, the first peak (P_1) is the main wave resulting from the blood ejected by left ventricle [60]. The tidal wave generated by the decrease of the ventricle blood pressure gives rise to the second peak (P_2), known as the point of inflection [59]. Subsequently, the ventricle becomes diastolic, and the aortic valve closes, leading to the reflection of the blood from the closed aortic valve and the formation of the last peak (P_3), which is the dicrotic wave. The radial artery augmentation index $AI_r = P_2/P_1$ and the radial diastolic augmentation $DAI = P_3/P_1$ can be derived from the acquired signals to obtain the heart rate with time delay $\Delta t_{DVP} = t_{(p1)} - t_{(p2)}$. The calculated AI_r, DAI, and Δt_{DVP} for our 30 year-old male participant, are 43%, 21%, and 250 ms respectively, which fall in the normal range for healthy males of the same age [61]. The demonstrated self-powered sensing capability to detect such small-scale biomechanical signals, together with the facile and low-cost manufacturing process, can potentially lead to broader applications of our devices for potential wearable biomedical devices.

In summary, we report a solution-based strategy for the scalable synthesis of chiral-chain piezoelectric tellurium nanowires with controlled diameters. The assembled Te nanowires by an LB approach are integrated into a wearable piezoelectric device, which can be conformably worn onto the human body, effectively converting the imperceptible time-variant mechanical vibration from the human body, e.g. radial artery pulse, into distinguishable electrical signals through straining the piezoelectric Te nanowires. We further revealed the process-structure-property relationship between the piezoelectric outputs from the integrated devices and the diameters of as-produced tellurium nanowires. The performance and efficiency of such a device can be optimized by controlling the process and the Te nanowire dimension. Our results suggest the potential of solution-synthesized Te nanowire as a new class of piezoelectric nanomaterial for self-powered devices. The intriguing piezoelectricity and semiconductor properties in Te nanowires with chiral-chain structures may lead to exciting opportunities in energy, piezotronics, and sensor applications [62–66].

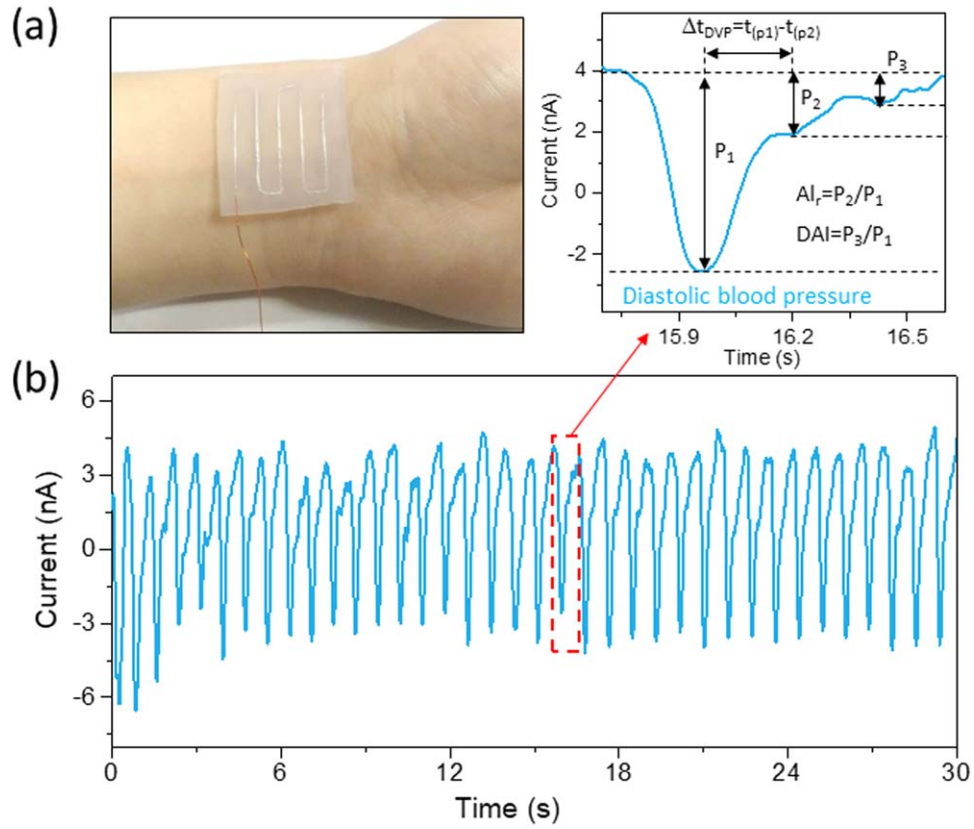

Figure 4. (a) Optical image of the wearable device attached on the human wrist. (b) The current output from the piezoelectric device for measuring the pulse on the wrist of a 30 year-old participant.

Materials and methods

Materials

PVP, hydrazine hydrate (85%, w/w), acetone, EG, aqueous ammonia solution (25%–28%, w/w), N, N-dimethylformamide (DMF), $CHCl_3$ were purchased from Sigma Aldrich. Na_2TeO_3 (97%) was purchased from Alfa Aesar. All chemical reagents were used without further purification. Double-distilled DI water was used for the synthesis.

Synthesis of Te nanowires

In the typical synthesis, Na_2TeO_3 and PVP was put into double-distilled water at room temperature with magnetic stirring to form a homogeneous solution. The resulting solution was poured into a Teflon-lined steel autoclave, which was then filled with aqueous ammonia solution and hydrazine hydrate. The autoclave was sealed and maintained at 180 °C for 3 h. Then the autoclave was cooled to room temperature naturally. The resulting blue products were precipitated by centrifuge at 5000 rpm for 5 min and washed with distilled water and acetone.

LB transfer of Te nanowires

The hydrophilic Te nanowires can be transferred to substrates by the LB technique. The washed Te nanowires were mixed with a certain volume ratio of N, N-dimethylformamide (DMF) and $CHCl_3$. Then the above solution was dropped into the DI water. After 30 min, the monolayer Te nanowire can be transferred to any substrates.

The effect of the reaction media for Te nanowire synthesis

The reduction reaction in acidic and alkaline environment can be formulated as follows:

$$TeO_3^{2-} + N_2H_5^+ + H^+ = Te + N_2 + 3H_2O \quad (1)$$

$$TeO_2^{2-} + N_2H_4 = Te + N_2 + H_2O + 2OH^-. \quad (2)$$

In acidic solution, the reaction comprises two half reactions:

$$TeO_3^{2-} + 6H^+ + 4e \rightarrow Te + 3H_2O \quad E^0 = 0.827\ eV \tag{3}$$

$$N_2H_5 + -4e \rightarrow N_2 + 5H^+ \quad E^0 = -0.23\ eV. \tag{4}$$

In alkaline solution:

$$TeO_3^{2-} + 3H_2O + 4e \rightarrow Te + 6OH^- \quad E^0 = -0.57\ eV \tag{5}$$

$$N_2H_4 + 4OH^- - 4e \rightarrow N_2 + 4H_2O \quad E^0 = -1.16\ eV. \tag{6}$$

From the equations (1) and (2), the standard EMF are 1.057 eV and 0.59 eV, respectively. This suggests that the reduction reaction in acidic media is much more rapidly than in alkaline media.

Device fabrication

The flexible piezoelectric device

A single layer of continuous thin LB film of horizontally-aligned Te nanowires was assembled on an ITO/PET flexible substrate (surface resistivity 60 Ω/sq) coated with a 1 μm thick PDMS. Finally, a 1 μm thick PDMS was spin-coated to cover the nanowire layer. The hydrophilic Te nanowire can be assembled without any additional treatment or functionalization.

The stretchable piezoelectric device

First, a layer of 1 μm silicone was deposited on the silicon wafer by spin coating. The LM was printed on the surface of the silicone by stage and syringe system. After connected the LM with copper wire, another layer of silicone was deposited to fix it. Then, the total electrode was peeled off from the silicon wafer.

Characterization

The thickness was determined by an AFM (Keysight 5500). High-resolution STEM/TEM imaging and SAED has been performed using a probe-corrected JEM-ARM 200 F (JEOL USA, Inc.) operated at 200 kV and EDS has been collected by an X-MaxN100TLE detector (Oxford Instruments). A field emission scanning electron microscope (Hitachi S-4800 Field Emission SEM) was used to characterize the morphologies of Te nanowires. A linear motor was applied as the external force to drive Te nanowire piezoelectric devices (operating distance, 20 mm; maximum speed, 1 m s^{-1}; acceleration, 1 m s^{-2}; deceleration, 1 m s^{-2}). Electrical measurements were done using an electrometer (Keithley 6514) and a low current preamplifier (Stanford Research System, SR570). All statistic data were summarized from three times of tests. For each type of sample, 10 peaks in total were applied to calculate average outputs and standard deviation.

Acknowledgments

WZW acknowledges the College of Engineering and School of Industrial Engineering at Purdue University for the startup support. WZW was partially supported by the National Science Foundation under grant CMMI-1762698. Part of the device fabrication was supported by a subcontract from the Idaho National Laboratory Directed Research and Development Program under DOE Idaho Operations Office Contract DE-AC07-05ID14517. The authors gratefully acknowledge the support and help from Professor Alexander Wei and his group in the LB assembly. QW and MJK were supported by the Louis Beecherl, Jr Endowment Funds.

Author contribution statement

WZW conceived and supervised the project. WZW and YXW designed the experiments. YXW synthesized the material. YXW and SW fabricated the devices. YXW and RXW performed the electrical and optical characterization. QW and MJK performed the TEM characterization. WZW and YXW analyzed the data. WZW and YXW wrote the manuscript. All authors have discussed the results and commented on the paper.

ORCID iDs

Wenzhuo Wu https://orcid.org/0000-0003-0362-6650

References

[1] Bouendeu E, Greiner A, Smith P J and Korvink J G 2011 A low-cost electromagnetic generator for vibration energy harvesting *IEEE Sens. J.* **11** 107–13
[2] Mitcheson P D, Miao P, Stark B H, Yeatman E M, Holmes A S and Green T C 2004 MEMS electrostatic micropower generator for low-frequency operation *Sensors Actuators* A **115** 523–9
[3] Fan F-R, Lin L, Zhu G, Wu W, Zhang R and Wang Z L 2012 Transparent triboelectric nanogenerators and self-powered pressure sensors based on micropatterned plastic films *Nano Lett.* **12** 3109–14
[4] Wang Z L and Song J H 2006 Piezoelectric nanogenerators based on zinc oxide nanowire arrays *Science* **312** 242–6
[5] Pradel K C, Wu W, Ding Y and Wang Z L 2014 Solution-derived ZnO homojunction nanowire films on wearable substrates for energy conversion and self-powered gesture recognition *Nano Lett.* **14** 6897–905
[6] Yang R, Qin Y, Dai L and Wang Z L 2009 Power generation with laterally packaged piezoelectric fine wires *Nat. Nanotechnol.* **4** 34–9
[7] Lee T I *et al* 2013 High-power density piezoelectric energy harvesting using radially strained ultrathin trigonal tellurium nanowire assembly *Adv. Mater.* **25** 2920–5
[8] Hwang G T *et al* 2014 Self-powered cardiac pacemaker enabled by flexible single crystalline PMN-PT piezoelectric energy harvester *Adv. Mater.* **26** 4880–7
[9] Fan F R, Tang W and Wang Z L 2016 Flexible nanogenerators for energy harvesting and self-powered electronics *Adv. Mater.* **28** 4283–305
[10] Wu W 2016 High-performance piezoelectric nanogenerators for self-powered nanosystems: quantitative standards and figures of merit *Nanotechnology* **27** 112503
[11] Datta A, Choi Y S, Chalmers E, Ou C and Kar-Narayan S 2017 Piezoelectric nylon-11 nanowire arrays grown by template wetting for vibrational energy harvesting applications *Adv. Funct. Mater.* **27** 1604262
[12] Kim S K, Bhatia R, Kim T-H, Seol D, Kim J H, Kim H, Seung W, Kim Y, Lee Y H and Kim S-W 2016 Directional dependent piezoelectric effect in CVD grew monolayer MoS_2 for flexible piezoelectric nanogenerators *Nano Energy* **22** 483–9
[13] Wu W *et al* 2014 Piezoelectricity of single-atomic-layer MoS_2 for energy conversion and piezotronics *Nature* **514** 470–4
[14] Wang X 2012 Piezoelectric nanogenerators—harvesting ambient mechanical energy at the nanometer scale *Nano Energy* **1** 13–24
[15] Nguyen V, Zhu R, Jenkins K and Yang R 2016 Self-assembly of diphenylalanine peptide with controlled polarization for power generation *Nat. Commun.* **7** 13566
[16] Qin Y, Wang X and Wang Z L 2008 Microfibre-nanowire hybrid structure for energy scavenging *Nature* **451** 809–13
[17] Zhao Y, Liao Q, Zhang G, Zhang Z, Liang Q, Liao X and Zhang Y 2015 High output piezoelectric nanocomposite generators composed of oriented $BaTiO_3$ NPs@PVDF *Nano Energy* **11** 719–27
[18] Kim K N, Chun J, Chae S A, Ahn C W, Kim I W, Kim S-W, Wang Z L and Baik J M 2015 Silk fibroin-based biodegradable piezoelectric composite nanogenerators using lead-free ferroelectric nanoparticles *Nano Energy* **14** 87–94
[19] Wang F, Jiang C, Tang C, Bi S, Wang Q, Du D and Song J 2016 High output nano-energy cell with piezoelectric nanogenerator and porous supercapacitor dual functions—a technique to provide sustaining power by harvesting intermittent mechanical energy from surroundings *Nano Energy* **21** 209–16
[20] Wu W, Wen X and Wang Z L 2013 Taxel-addressable matrix of vertical-nanowire piezotronic transistors for active and adaptive tactile imaging *Science* **340** 952–7
[21] Wang Z L 2017 On Maxwell's displacement current for energy and sensors: the origin of nanogenerators *Mater. Today* **20** 74–82
[22] Chen C Q and Zhu J 2007 Bending strength and flexibility of ZnO nanowires *Appl. Phys. Lett.* **90** 043105
[23] Li P *et al* 2014 *In situ* transmission electron microscopy investigation on fatigue behavior of single ZnO wires under high-cycle strain *Nano Lett.* **14** 480–5
[24] Qi Y, Jafferis N T, Lyons K, Lee C M, Ahmad H and McAlpine M C 2010 Piezoelectric ribbons printed onto rubber for flexible energy conversion *Nano Lett.* **10** 524–8
[25] Chang C, Tran V H, Wang J, Fuh Y-K and Lin L 2010 Direct-write piezoelectric polymeric nanogenerator with high energy conversion efficiency *Nano Lett.* **10** 726–31
[26] Hu Y, Zhang Y, Xu C, Zhu G and Wang Z L 2010 High-output nanogenerator by rational unipolar assembly of conical nanowires and its application for driving a small liquid crystal display *Nano Lett.* **10** 5025–31
[27] Long L, Chen-Ho L, Youfan H, Yan Z, Xue W, Chen X, Robert L S, Lih J C and Zhong Lin W 2011 High output nanogenerator based on assembly of GaN nanowires *Nanotechnology* **22** 475401
[28] Xu S, Qin Y, Xu C, Wei Y, Yang R and Wang Z L 2010 Self-powered nanowire devices *Nat. Nanotechnol.* **5** 366
[29] Hu Y, Zhang Y, Xu C, Lin L, Snyder R L and Wang Z L 2011 Self-powered system with wireless data transmission *Nano Lett.* **11** 2572–7
[30] Wang Z L 2017 On Maxwell's displacement current for energy and sensors: the origin of nanogenerators *Mater. Today* **20** 74–82
[31] von Hippel A 1948 Structure and conductivity in the VIb group of the periodic system *J. Chem. Phys.* **16** 372–80
[32] Cherin P and Unger P 1967 The crystal structure of trigonal selenium *Inorg. Chem.* **6** 1589–91
[33] Mayers B T, Liu K, Sunderland D and Xia Y 2003 Sonochemical synthesis of trigonal selenium nanowires *Chem. Mater.* **15** 3852–8
[34] Wang Y *et al* 2018 Field-effect transistors made from solution-grown two-dimensional tellurene *Nat. Electron.* **1** 228–36
[35] Royer D and Dieulesaint E 1979 Elastic and piezoelectric constants of trigonal selenium and tellurium crystals *J. Appl. Phys.* **50** 4042–5
[36] Arlt G and Quadflieg P 1969 Electronic displacement in tellurium by mechanical strain *Phys. Status Solidi* b **32** 687–9
[37] Peng H, Kioussis N and Snyder G J 2014 Elemental tellurium as a chiral *p*-type thermoelectric material *Phys. Rev.* B **89** 195206
[38] Coker A, Lee T and Das T 1980 Investigation of the electronic properties of tellurium—energy-band structure *Phys. Rev.* B **22** 2968
[39] Gao S, Wang Y, Wang R and Wu W 2017 Piezotronic effect in 1D van der Waals solid of elemental tellurium nanobelt for smart adaptive electronics *Semicond. Sci. Technol.* **32** 104004
[40] Bae S *et al* 2010 Roll-to-roll production of 30 inch graphene films for transparent electrodes *Nat. Nanotechnol.* **5** 574
[41] Liu J-W, Xu J, Liang H-W, Wang K and Yu S-H 2012 Macroscale ordered ultrathin telluride nanowire films, and tellurium/telluride hetero-nanowire films *Angew. Chem., Int. Ed. Engl.* **51** 7420–5
[42] Lan W-J, Yu S-H, Qian H-S and Wan Y 2007 Dispersibility, stabilization, and chemical stability of ultrathin tellurium nanowires in acetone: morphology change, crystallization, and transformation into TeO2 in different solvents *Langmuir* **23** 3409–17
[43] Qian H-S, Yu S-H, Gong J-Y, Luo L-B and Fei L-F 2006 High-quality luminescent tellurium nanowires of several nanometers in diameter and high aspect ratio synthesized by a poly (vinyl pyrrolidone)-assisted hydrothermal process *Langmuir* **22** 3830–5
[44] Zasadzinski J A, Viswanathan R, Madsen L, Garnaes J and Schwartz D K 1994 Langmuir-blodgett films *Science* **263** 1726
[45] Liu Z, Li S, Yang Y, Hu Z, Peng S, Liang J and Qian Y 2003 Shape-controlled synthesis and growth mechanism of one-dimensional nanostructures of trigonal tellurium *New J. Chem.* **27** 1748–52

[46] Jirgensons B 1952 Solubility and fractionation of polyvinylpyrrolidone *J. Polym. Sci.* **8** 519–27
[47] Liu J-W, Wang J-L, Wang Z-H, Huang W-R and Yu S-H 2014 Manipulating nanowire assembly for flexible transparent electrodes *Angew. Chem., Int. Ed. Engl.* **53** 13477–82
[48] Liu J, Fei P, Zhou J, Tummala R and Wang Z L 2008 Toward high output-power nanogenerator *Appl. Phys. Lett.* **92** 173105
[49] Agrawal R and Espinosa H D 2011 Giant piezoelectric size effects in zinc oxide and gallium nitride nanowires. a first principles investigation *Nano Lett.* **11** 786–90
[50] Qin C, Gu Y, Sun X, Wang X and Zhang Y 2015 Structural dependence of piezoelectric size effects and macroscopic polarization in ZnO nanowires: a first-principles study *Nano Res.* **8** 2073–81
[51] Wei B, Zheng K, Ji Y, Zhang Y, Zhang Z and Han X 2012 Size-dependent bandgap modulation of ZnO nanowires by tensile strain *Nano Lett.* **12** 4595–9
[52] Li M and Li J C 2006 Size effects on the band-gap of semiconductor compounds *Mater. Lett.* **60** 2526–9
[53] He R and Yang P 2006 Giant piezoresistance effect in silicon nanowires *Nat. Nanotechnol.* **1** 42
[54] Shi B, Zheng Q, Jiang W, Yan L, Wang X, Liu H, Yao Y, Li Z and Wang Z L 2016 A packaged self-powered system with universal connectors based on hybridized nanogenerators *Adv. Mater.* **28** 846–52
[55] Hu Y and Wang Z L 2015 Recent progress in piezoelectric nanogenerators as a sustainable power source in self-powered systems and active sensors *Nano Energy* **14** 3–14
[56] Chun J, Kang N-R, Kim J-Y, Noh M-S, Kang C-Y, Choi D, Kim S-W, Lin Wang Z and Min Baik J 2015 Highly anisotropic power generation in piezoelectric hemispheres composed stretchable composite film for self-powered motion sensor *Nano Energy* **11** 1–10
[57] Xu S, Qin Y, Xu C, Wei Y, Yang R and Wang Z L 2010 Self-powered nanowire devices *Nat. Nano* **5** 366–73
[58] Kubo M, Li X, Kim C, Hashimoto M, Wiley B J, Ham D and Whitesides G M 2010 Stretchable microfluidic radiofrequency antennas *Adv. Mater.* **22** 2749–52
[59] Schwartz G, Tee B C K, Mei J, Appleton A L, Kim D H, Wang H and Bao Z 2013 Flexible polymer transistors with high pressure sensitivity for application in electronic skin and health monitoring *Nat. Commun.* **4** 1859
[60] Park J, Kim M, Lee Y, Lee H S and Ko H 2015 Fingertip skin–inspired microstructured ferroelectric skins discriminate static/dynamic pressure and temperature stimuli *Sci. Adv.* **1** e1500661
[61] Nichols W W 2005 Clinical measurement of arterial stiffness obtained from noninvasive pressure waveforms *Am. J. Hypertension* **18** 3S–0S
[62] Wu W and Wang Z L 2016 Piezotronics and piezo-phototronics for adaptive electronics and optoelectronics *Nat. Rev. Mater.* **1** 16031
[63] Wu W, Pan C, Zhang Y, Wen X and Wang Z L 2013 Piezotronics and piezo-phototronics—from single nanodevices to array of devices and then to integrated functional system *Nano Today* **8** 619–42
[64] Wang Z L 2010 Piezopotential gated nanowire devices: piezotronics and piezo-phototronics *Nano Today* **5** 540–52
[65] Wang Z L 2012 *Piezotronics and Piezo-Phototronics* (Berlin: Springer)
[66] Wang Z L 2007 Nanopiezotronics *Adv. Mater.* **19** 889–92